Appl. Phys. B 67, 497–504 (1998)

Applied Physics B
Lasers
and Optics

Detection of aromatic pollutants in the environment by using UV-laser-induced fluorescence

P. Karlitschek, F. Lewitzka, U. Bünting, M. Niederkrüger, G. Marowsky

Laser Laboratorium Göttingen e.V., P.O. Box 2619, D-37016 Göttingen, Germany
(Fax: +49-551/5035-99, E-mail: pkarlit@llg.gwdg.de)

Received: 19 March 1998/Revised version: 2 June 1998

Abstract. We present a compact and mobile battery-operated laser induced fluorescence (LIF) system. It is based on a diode-pumped solid-state laser with UV frequency conversion and a 7-ns pulse duration. The third (355 nm) and fourth (266 nm) harmonics of the laser can be used alternately. The detection system consists of a polychromator, a gated image intensifier, and a CCD camera, which can acquire time-resolved spectra with nanosecond time resolution.

Fluorescence spectra, decay times, and detection limits of the 16 US-EPA polycyclic aromatic hydrocarbons (PAH) have been measured and the results are discussed in terms of separability of single PAHs in a multicomponent mixture. The results of a mathematical analysis of a 16-component mixture is presented. Spectra from natural water samples contaminated with gasoline and tar are also presented and the potential and limits of the LIF technique are discussed.

PACS: 42.60B; 42.80; 82.80

Environmental problems have attracted increasing attention in the past decade. The United States Environmental Protection Agency (US-EPA) has assigned a number of substances as priority pollutants. Among them, polycyclic aromatic hydrocarbons (PAHs) and mono-aromatics [benzene, toluene, xylene, ethylbenzene (BTXE)] play an important role due to their mutagenic and/or carcinogenic potential. PAHs are generated in any incomplete combustion process. The soil near gasworks or tar production plants is also frequently contaminated with PAHs. Monoaromatics (at trace levels also PAHs) are constituents of mineral oil products. Thus after oil spills, they can contaminate soil, surface water and, due to their high mobility, also groundwater.

Excellent laboratory techniques exist for the selective analysis of PAH and BTXE. But these techniques are very expensive if a continuous monitoring is desired or if hundreds of soil samples have to be analyzed to asses the hazard potential of an old gasworks location. For these applications, field techniques are needed that permit high sample throughput at low cost per analysis. Since field techniques are expected to be less accurate and less selective than laboratory methods, they must be regarded as an additional tool in environmental analysis.

Spectroscopic techniques are well suited for this purpose since they permit, per se, a continuous measurement. In conjunction with fiber optics, the construction of on-site and in situ measurement systems is feasible. The application of laser-induced fluorescence spectroscopy for the analysis of BTXE and PAHs has several advantages: (i) laser light can be effectively coupled into optical fibers; (ii) these molecules have large absorption cross sections in the UV and exhibit high fluorescence quantum yields; (iii) if pulsed lasers are used, fluorescence decay curves can be recorded which reveal additional information. The last point is regarded as very important since multi-component mixtures must be analyzed in environmental analysis without the aid of pre-cleaning steps from laboratory analysis.

These advantages have led to the development of a variety of laboratory and field instruments [1–10]. Some of them employ a nitrogen laser (337 nm) while others a flash-lamp-pumped Nd:YAG laser. Our goal was to develop an instrument which is battery powered and can be operated at two UV wavelengths, namely 266 nm and 355 nm. The 266-nm wavelength is essential if monoaromatics and small polyaromatic compounds have to be analysed. The 355-nm wavelength should help to selectively excite some larger PAH molecules. Since commercially available pulsed UV laser sources are not well suited for field sensor applications, (because of weight, size, need of water cooling, high energy consumption, price), we have developed a laser system that meets all requirements.

The use of UV LIF in combination with fiber-optic sensing is still restricted by the transmission properties of fused silica optical fibers in the UV range. Our results concerning the fibers have been published elsewhere [11–15]. We present here the set-up of a fiber-optic instrument that consists of a diode-pumped solid-state laser with upconversion into the UV, an optimized fiber-optic probe and a temporally and spectrally resolved detection unit (see Fig. 1). We also

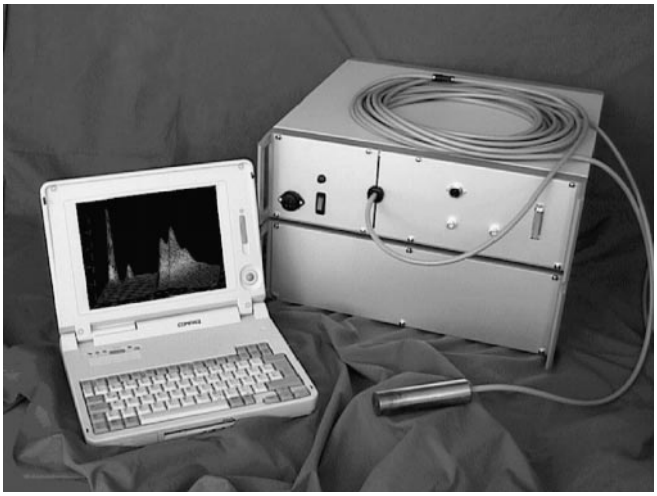

Fig. 1. Photograph of the fiber-optic LIF instrument consisting of two 19″ cases containing a pulsed diode-pumped Nd:YAG laser with frequency conversion into the UV, and an optical multichannel analyzer. The system is controlled by a laptop PC via the parallel port. The fiber-optic probe with 15-m-long cable is also shown

present and discuss the experimental results obtained with this system.

1 Experimental set-up of a mobile LIF system

The schematic set-up of our fiber-optic LIF system is shown in Fig. 2. The principal components are a pulsed UV laser as the excitation source, a fiber-optic probe, a detection unit for temporally and/or spectrally resolved detection of the fluorescence light, and the control and data acquisition unit. Time resolution in the nanosecond range is considered necessary for the separation of fluorescence of the aromatic molecules from the natural background fluorescence. Therefore, a nanosecond-pulsed light source and a fast detection unit is needed. For field applications, a flexible sensor design is necessary to allow in situ measurements. This is accomplished by using a fiber-optic cable for beam delivery. Furthermore, the constraints for a mobile system have to be met, i.e. compact and rugged design, low power consumption, and independence from water and power installation requirements. These demands led to the development of a specialized diode-pumped solid-state laser as the excitation source.

1.1 Diode-pumped frequency upconverted solid-state laser

To meet the requirements for LIF detection, a nanosecond-pulsed UV laser is necessary. Unfortunately, only a few fixed-frequency lasers are available in the UV. In the wavelength range of interest, these are the excimer lasers at 248 and 308 nm and the nitrogen laser at 337 nm. Different wavelengths may also be generated by nonlinear processes from other lasers, such as either dye or solid-state lasers. Several LIF field instruments based on nitrogen lasers have been reported [1–3, 6–8], since compact and reliable commercial N_2 lasers are available. Frequency-upconverted flashlamp-pumped solid-state lasers have been used mainly in the laboratory. Lieberman et al. have reported on a truck-mounted system for field applications [9].

The progress in the field of high-power laser diodes and laser diode arrays has led to the construction of efficient solid-state lasers using these devices as pumping sources [16]. This technology readily allows the construction of a specialized laser system that fulfils the requirements for an excitation source for our laser fluorimeter. In particular, the fourth harmonic (266 nm) of the Nd:YAG lasers is well suited, since the absorption of aromatic molecules is high at around 260 nm. The requirements for the system were as follows: pulse duration less than 10 ns for time-resolved studies, pulse energies of 50–100 μJ in the UV (limited by the UV transmission properties of optical fibers), moderate repetition rate (50–100 Hz), low average power consumption (battery operation), and thermoelectric cooling. Commercial laser systems that meet these requirements are not available, mostly due to longer pulse length. This led to the construction of a specialized laser system, which is described in [17].

We use a single laser diode array in the end-pumping configuration, since this has proven advantageous in the medium power range [18]. In the set-up shown in Fig. 3, a high-power quasi-CW diode array (SDL-3231-A4) with 240 W of peak power and a 2% duty cycle was used as the pump source. The array consists of four bars with emitting areas of 10 mm × 1 μm and a spacing of 0.4 mm between the bars. The pump

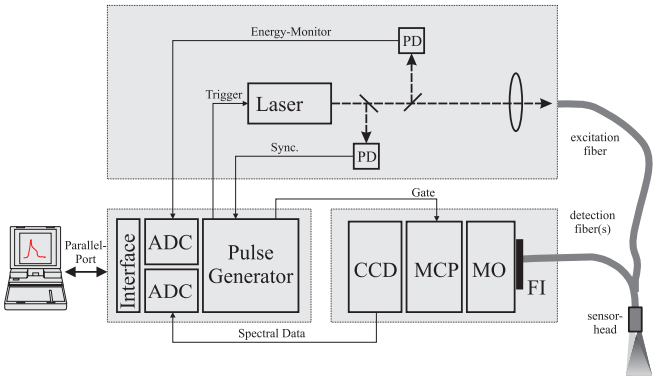

Fig. 2. Schematic drawing of our fiber-optic LIF instrument for in situ detection of water pollutants. PD: Photodiodes. FI: edge filter. MO: monochromator. MCP: multichannel plate image intensifier. CCD: slow-scan CCD-line camera. ADC: analog-to-digital converters

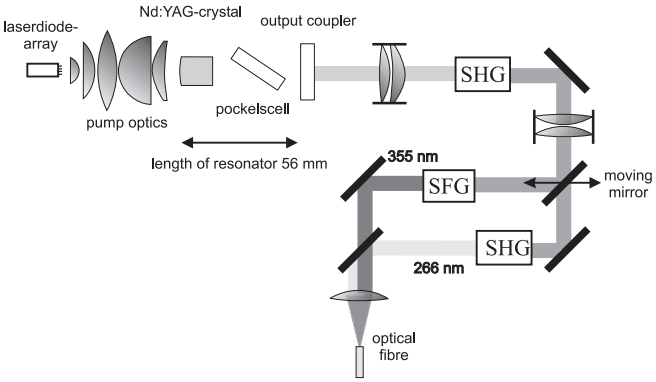

Fig. 3. Setup of the excitation laser source with switchable frequency-conversion unit. The moving mirror allows one to switch between 355 nm and 266 nm radiation to be coupled into the fiber

beam was shaped by cylindrical optics and then focused into the laser crystal. The pump spot is approximately 2 mm × 1 mm (FWHM). The pump array is mounted on a thermoelectric cooler and kept at an optimum temperature to match the absorption of the crystal. One side of the crystal has a 100-mm radius of curvature and is AR-coated for the pump and HR-coated for the laser wavelength. This mirror and a flat output coupler form a cavity which is only 56 mm long. Different output coupler reflectivities were tested for performance optimization, which finally led to an optimum value of 70%. With this short cavity, the laser beam was multi-mode with 50% of the energy in the TEM_{00} mode.

For the generation of nanosecond pulses, a KDD*P Pockels cell cut at Brewster's angle was inserted into the cavity to actively Q-switch the laser. With a pump duration of 300 μs, we obtained pulses of 2.5 mJ energy and 9 ns duration at the fundamental wavelength of 1064 nm in a multimode beam. The beam quality in the *x* direction (parallel to the Pockels cell surface) remains the same as that without Pockels cell, but it is reduced in the *y* direction.

For the generation of UV pulses, the radiation of the laser is first upconverted to 532 nm. The beam passes a half-wave plate and is then focused into a 5-mm-long KTP crystal cut for type-II phase-matching. Energies of 1 mJ in 8 ns were obtained in the green (40% efficiency). The wave plate was used to rotate the polarisation so that the high divergence direction of the 1064-nm beam corresponds to the noncritical phase-matching direction of the crystal.

The UV radiation is generated in a second step. The upconversion unit consists of a sum frequency generation (SFG) path for the generation of 355-nm radiation and a second-harmonic generation (SHG) path for the generation of 266-nm radiation. A dielectric mirror (HR 532 and 1064, 45°) mounted on a motorized translation stage allows one to switch between the two beam paths (see Fig. 3). If the mirror is moved into the beam, 532 and 1064 nm radiation is focused into a 7-mm-long BBO crystal (type-I phase-matching) after it passed a dual-λ half-wave plate (532 nm for λ/2 retardation, 1064 nm for λ retardation) for polarization matching. The emitted 355-nm radiation is bent with a dielectric mirror (HR 355 nm, 45°), passes a beam-combining dielectric mirror (AR 355 nm, HR 266 nm, 45°), focused again and coupled into a SMA-905 fiber connector. The alternative beam path, when the moving mirror is moved out of the 532 and 1064 nm beams, is bent by a dielectric mirror (HR 532, 45°) and focused into a second 7-mm-long BBO crystal (type-I phase-matching). The beam-combining mirror guides the beam through the same coupling optics as the 355-nm beam and into the same fiber. Thus, the laser unit allows one to switch between 266-nm and 355-nm pulses and couples them into a single fiber. At 355 nm, pulses of up to 180 μJ/7 ns were generated, whereas at 266 nm up to 140 μJ/7 ns were obtained (see Table 1).

Table 1. Performance data of the Nd:YAG laser system at 100 Hz

Wavelength	Pulse energy	Pulse duration
Fundamental (1064 nm)	2.5 mJ	9 ns
2nd harmonic (532 nm)	870 μJ	8 ns
3rd harmonic (355 nm)	180 μJ	7 ns
4th harmonic (266 nm)	140 μJ	7 ns

1.2 Fiber-optic probe design

In general, two different geometries for the design of a fiber-optic LIF sensor are possible. Either excitation and fluorescence light are guided through the same fiber or multiple fibers are used. The realization of the first geometry requires one to separate the excitation light from fluorescence, which is many orders of magnitude weaker in intensity. A second disadvantage is the fluorescence emission and Raman scattering of the fiber itself, which is induced by the laser radiation. The advantage of this geometry is the perfect overlap of the exit and entrance cones of the excitation and detection fibers. The second geometry lacks this perfect overlap and has to be optimized for the turbidity of the medium. We have performed both numerical and experimental optimization of the fiber distance and angle [19]. The results of this optimization indicate that, as expected, the distance has to be kept as small as possible. It follows that a design with several detection fibers with the same cross section as a single thick fiber should be more efficient, since the surface area of the detection fibers is on average closer to the excitation fiber. The whole cable is more flexible with thinner fibers, too. We have chosen a design with four 400-μm detection fibers around a 600-μm excitation fiber. The optimal angle between excitation and detection fibers varies between 10 and 30°, depending on the turbidity of the water. We have chosen a value of 20° that is good for low to medium turbidity [19].

The design of the fiberoptic probe is shown in Fig. 4. The total cable length is 15 m. The transmission at 266 nm is about 50% for a laser intensity of 2 MW/cm^2 corresponding to a transmission of 95.6%/m (more details in [14, 15]). Photodegradation (UV-induced damage) is negligible at this intensity [14].

One end of the cable consists of the optrode where the fibers are fixed close together at 20° angle. At the other end the cable splits up into one arm containing the 600 μm fiber

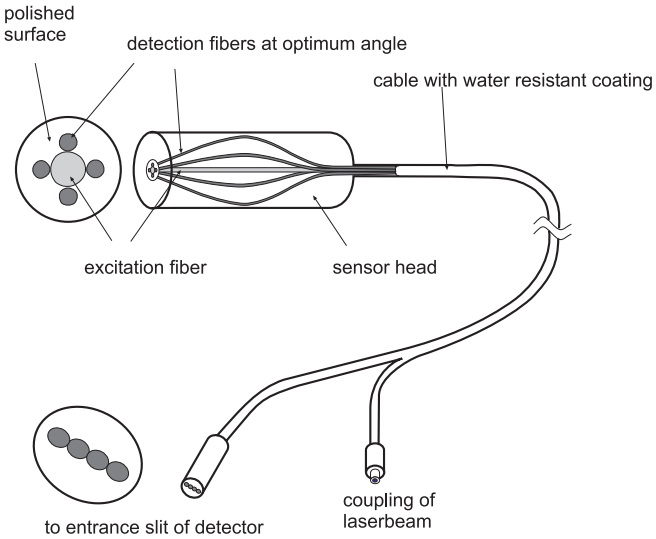

Fig. 4. Complete fiber-optic probe with cable

that is fixed with a SMA 905 connector to the laser and a second arm connected to the spectrometer where the four fibers are lined up to match the entrance slit of the polychromator.

1.3 Set-up of the detection unit

The detection unit was realized as an optical multichannel analyser with a time resolution of 5 ns. The set-up is shown schematically in Fig. 2. The fluorescence light that is collected and transmitted by the detection fibers is coupled into a 140-mm monochromator with holographic grating (f number 2, 285 lines/mm, blaze wavelength 285 nm, dispersion 24.2 nm/mm). The fibers (400 μm diameter) are arranged in a line in front of the entrance. This kind of coupling is more efficient than with imaging optics, even if the fiber diameter is larger than the slit width. The spectral resolution is determined by the entrance slit (6 nm for 250 μm slit width) over a spectral range from 250 to 530 nm.

At the exit focal plane of the polychromator is an image intensifier with an S20 photocathode that allows short gating (down to 5 ns) and variable amplification of the fluorescence light. 1 : 1 imaging optics is used to couple the image intensifier with a cooled slow-scan CCD camera (Hamamatsu C-5809). The 512×64-element chip is operated in the binning mode as a 512-element line camera. In this mode the readout rate is 100 spectra per second with a high dynamic range of 1 : 20000. A 16-bit AD converter card with FIFO memory is coupled to a laptop PC via the parallel port. A second card contains the timing unit that allows the generation of a variable 5–250-ns-long gate pulse for the image intensifier. The gate can be shifted relatively to the laser pulse with 1 ns time resolution. To prevent inaccuracies due to a possible jitter of the laser, the timing unit is synchronized by means of a photodiode on the emitted laser pulse. The propagation delay of the timing unit is compensated by the delay of the light in the optical fibers.

A second photodiode serves as a monitor of the laser energy. Every single spectrum acquired is normalized to this monitor signal. Any change in transmission through the fibers is compensated by normalization of a whole time-resolved spectrum to the Raman signal, which is proportional to the incident laser energy.

2 Measurements

2.1 Fluorescence of PAH and BTX molecules

The fluorescence of PAH and BTXE molecules was investigated with 266 nm excitation. Solutions of 10 μg/l PAH molecules in water were prepared with certified chemicals (Promochem, Germany) to determine the fluorescence decay curves. As an example the spectrum of benzo(a)pyrene is shown in Fig. 5. In this figure, two possible representations of the time-resolved spectra are shown: (a) a 3-D plot of intensity versus wavelength and time (b) a contour plot of the same data. A typical signal in each spectrum is the Raman peak of the H_2O molecule at 294 nm. The strong 266-nm Rayleigh-scattering peak is damped by a cut-off filter and the wavelength range of the detector is shifted to exclude the peak from registration. It also shows up at 532 nm as the second

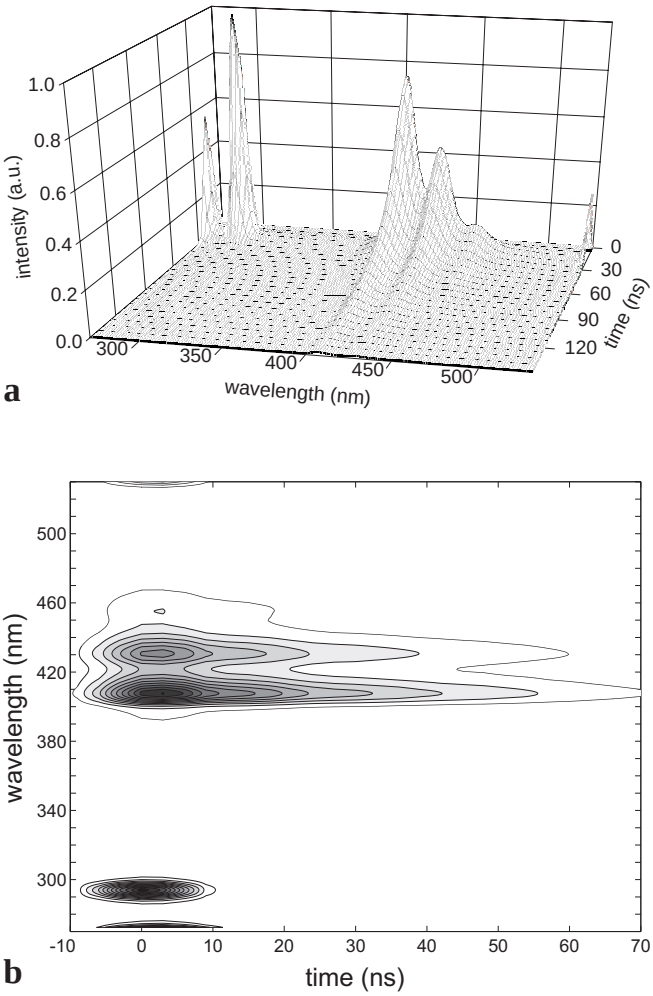

Fig. 5a,b. Time-resolved fluorescence spectrum of 10 μg/l benzo(a)pyrene in distilled water. **a** 3-dimensional plot of the data; **b** contour plot of the data

diffraction order of the grating. It is one order of magnitude weaker than the first-order scattering signal. The Raman signal is used for energy calibration, since the intensity of the peak is proportional to the incident radiation into the sample. The Rayleigh-scattering signal can be used as a measure of turbidity of the sample, because additional scattering particles lead to an increase in the signal due to Mie scattering. The fluorescence signal can be observed between 270 and 532 nm.

We recorded the time-resolved spectra of the 12 strong fluorescing PAHs from the US-EPA list. In order to determine decay times, the spectra were evaluated beginning with the moment when the laser pulse is over. A least-squares fit of an exponential function to our decay curves then yielded the individual decay time for each molecule. Alternatively a Knorr–Harris fit (see next section) with a single component was performed on the data. The results are presented together in Table 2. The decay times are also depicted in Fig. 6, where they are plotted against the wavelength range of maximum fluorescence. From this figure, it follows that there is only pyrene with a very long decay time of 122 ns. Most of the other molecules have decay times between 24 and 40 ns. Only benzo(k)fluoranthene, fluorene, and anthracene have shorter decay times. The decay times play an important role for the discrimination of the background fluorescence and for the

Table 2. Decay times for 12 single PAHs obtained by a least-squares fit to our experimental data compared with the values obtained by a single component Knorr–Harris fit. Standard deviations of several fits at different wavelenghts are given as an estimation of error for the least-squares fit

Substance	Decay time (ns) Exp. fit	Std. Dev. (ns)	Decay time (ns) Knorr–Harris fit
Acenaphtene	24.0	0.7	26
Anthracene	3.8	1.0	3.8
Benzo(a)anthracene	26.1	0.3	26
Benzo(k)fluoranthene	9.7	0.5	9
Benzo(b)fluoranthene	34.8	1.5	31
Benzo(a)pyrene	27.6	0.7	28
Chrysene	26.4	1.5	26
Fluoranthene	32.5	1.0	33
Fluorene	5.0	1.0	5
Naphtalene	36.7	0.4	37
Phenanthrene	36.8	0.4	37
Pyrene	122.2	3	125

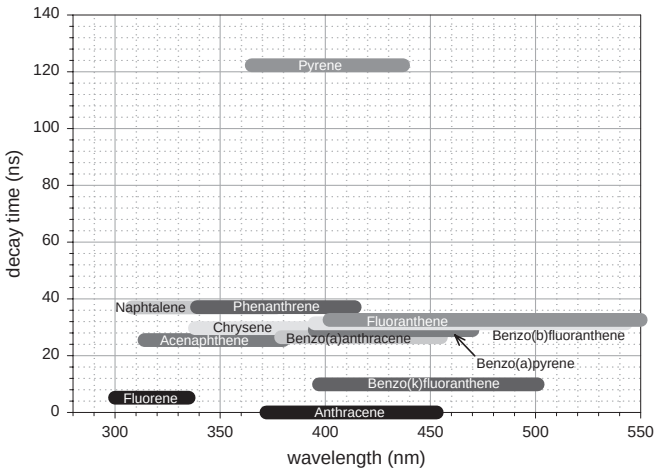

Fig. 6. Measured decay times of 12 PAHs plotted against their fluorescence wavelength range (> 10% of peak intensity). Excitation wavelength was 266 nm

separation of mixtures that is explained in the next section. Since natural waters contain humic acids, which also exhibit strong fluorescence with short decay times of less than 10 ns when excited by UV radiation, molecules with longer decay times can be distinguished better from the background signal.

Relative fluorescence intensities were determined with the above-mentioned 10 μg/l solutions. Detection limits were estimated from the relative peak intensities by dividing the signal counts of the peak heights by a value of 50. This value corresponds to three times the counts of the blank signal, which still allows comparison of the contours of the time-resolved spectra.

These estimated detection limits do not account for any fluorescence from humic material that influences the signal in natural waters. They are simply a measure of the quantum efficiency of the fluorescence process and of the absorption cross section at the excitation wavelength. 12 out of the 16 PAH of the US-EPA list of priority pollutants exhibit strong fluorescence when excited with 266-nm radiation (see Table 3). In contrast to a nitrogen laser at 337 nm, this source is not only able to excite the four- and five-ring aromatic molecules but also the smaller ones like naphtalene, acenaphthene and even the BTXE monoaromatics. The detection limits in distilled water for most of the PAH molecules are within the order of magnitude of the sum value for PAHs according to the US-EPA list and other regulations.

Table 3. Estimation of detection limits and regulation limits. All values are given in μg/l. Summed values are marked with a * sign. TVO-BRD: German drinking water regulation. WHO: drinking water regulation of the World Health Organization. EPA: US Environment Protection Agency (USA) "priority pollutants" drinking water limits. DVGW-OW: regulation limits for water used for drinking water production (Deutscher Verein von Gas- und Wasserfachmännern)

Substance	detection limit	Regulation limits			
		TVO-BRD	WHO	EPA	DVGW-OW
Fluorene	0.01	–	–	0.2*	3.0*
Benzo(a)pyrene	0.02	0.2*	0.7	0.2*	3.0*
Benzo(a)anthracene	0.03	–	–	0.2*	3.0*
Chrysene	0.08	–	–	0.2*	3.0*
Acenaphthene	0.08	–	–	0.2*	3.0*
Benzo(k)fluoranthene	0.08	0.2*	–	0.2*	3.0*
Pyrene	0.2	–	–	0.2*	3.0*
Anthracene	0.1	–	–	0.2*	3.0*
Benzo(b)fluoranthene	0.1	0.2*	–	0.2*	3.0*
Phenanthrene	0.2	–	–	0.2*	3.0*
Naphtalene	0.3	–	–	0.2*	3.0*
Fluoranthene	0.4	0.2*	–	0.2*	3.0*
Phenol	1	0.5	–		10
Xylene	10	10	500		20
Toluene	50	10	700		20
Benzene	100	10	10		20

3 Analysis of multicomponent spectra

For practical applications, it is often essential to determine individual species of mixtures. In a complex mixture it is therefore necessary to take all of the available information as wavelength- and time-resolved fluorescence signal and the two excitation wavelengths into account. To demonstrate a suitable method for the decomposition, we measured the time-resolved spectra of a 16-component mixture of PAHs according to the US-EPA standard 610 (from Promochem, Germany) with both excitation sources. The spectra are shown in Figs. 7 and 8. From our previous experiments, we know that only 12 of the 16 PAH show significant fluorescence signal, so that we have in fact a 12-component mixture. To further process the signal, we used the chemometrical approach first described by Knorr and Harris [20, 21].

The data matrix **D** corresponding to a time-resolved emission spectrum of a single component can be expressed as the scalar product of a row vector, describing the temporal behavior and a column vector, describing the spectral behavior of the fluorescence. In mixtures, the data matrix is made up by a set of row and column vectors, one pair of row and column vectors for each component:

$$\mathbf{D} = \boldsymbol{R} \times \boldsymbol{C} \ ,$$

The goal of the subsequent analysis is to calculate these row and column vectors of a given matrix. Since fluorescence decay can be described by exponential functions, one parameter

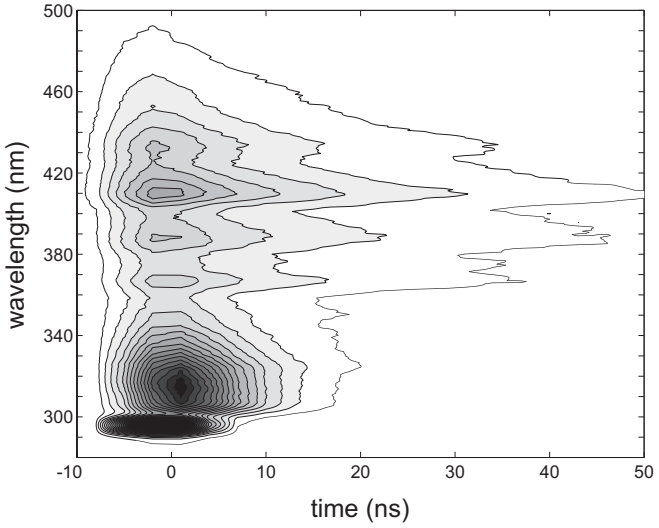

Fig. 7. Contour plot of the time resolved fluorescence spectrum of an EPA-610 standard containing the 16 PAHs of the US-EPA list of priority pollutants. Excitation wavelength: 266 nm

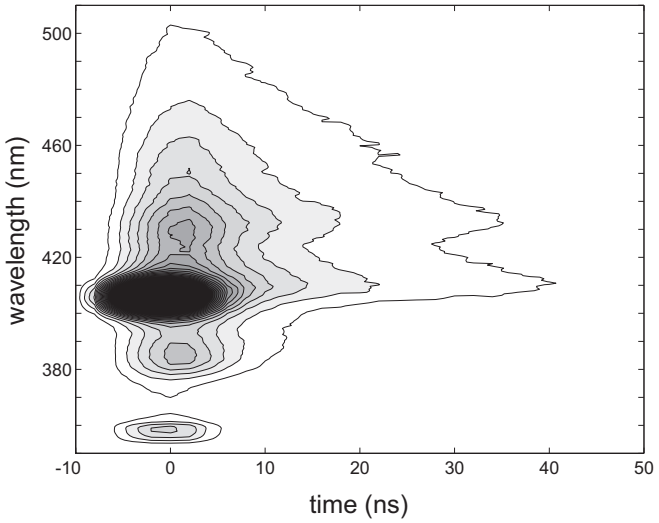

Fig. 8. Contour plot of the time-resolved fluorescence spectrum of an EPA-610 standard containing the 16 PAHs of the US-EPA list of priority pollutants. Excitation wavelength: 355 nm

per component – the time constant – is sufficient to describe the temporal behaviour ($\boldsymbol{R}_{\text{test}}$). The corresponding spectral vectors $\boldsymbol{C}$ are calculated by $\boldsymbol{C} = \mathbf{D} \times (\boldsymbol{R}_{\text{test}})^{+}$, where $(^{+})$ denotes the pseudo inverse. It is possible to model the data matrix **D** by optimizing only the time constants [20, 21]. In complex multicomponent mixtures, not all individual components can be separated. A data matrix can typically be reconstructed by three (abstract) components. Then each 'single component spectrum' can be a superposition of two or more spectra.

The results of a three component Knorr–Harris fit of the 266-nm excited spectrum can be seen in Fig. 9. The shortest decaying component from 300 to 350 nm is easily identified as fluorene with a decay time of 5 ns. A weak signal from 400 to 480 nm can also be seen (benzo(k)fluoranthene). The longest decaying component consists mainly of pyrene with a 122 ns decay time, but it is not fully separated from the

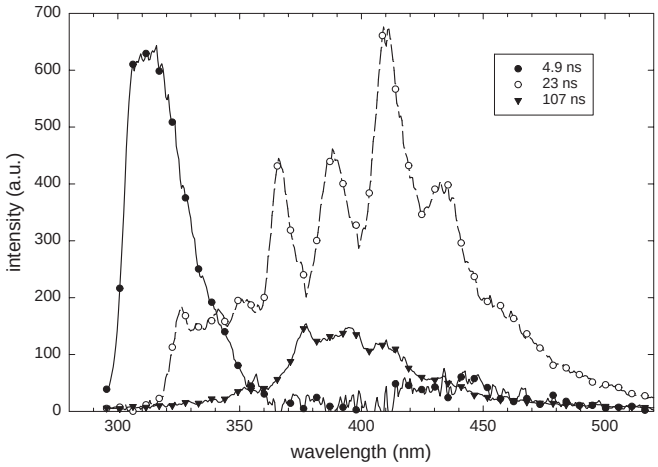

Fig. 9. Plot of the three components obtained by a Knorr–Harris fit applied to the time-resolved spectrum of the US-EPA 610 standard. Excitation wavelength: 266 nm

component with a 23 ns decay time, which leads to a decay time of 107 ns for this component according to the fit. The 23-ns component contains most of the PAHs. At least five individual molecules can be identified owing to their characteristic spectrum (see Fig. 10). A six-component least-squares fit yielded very good coincidence with the measured spectrum; acenaphthene (325/340 nm), benzo(a)anthracene (390/410 nm), benzo(a)pyrene (410/430 nm), chrysene (365/380 nm), and phenanthrene (350/370 nm) are obviously identified due to their characteristic peaks, and the mixture benzo(b)fluoranthene/fluoranthene because of its long wavelength. Since these two molecules have nearly identical spectra, they cannot be separated from each other. Naphthalene has spectral properties similar to those of acenaphtene but has much weaker fluorescence, so that it cannot be separated although the decay times differ significantly (37 and 25 ns).

The 355-nm excited spectrum was also decomposed into three components (Fig. 11). Since much less PAHs can be excited by 355-nm radiation, the identification of single com-

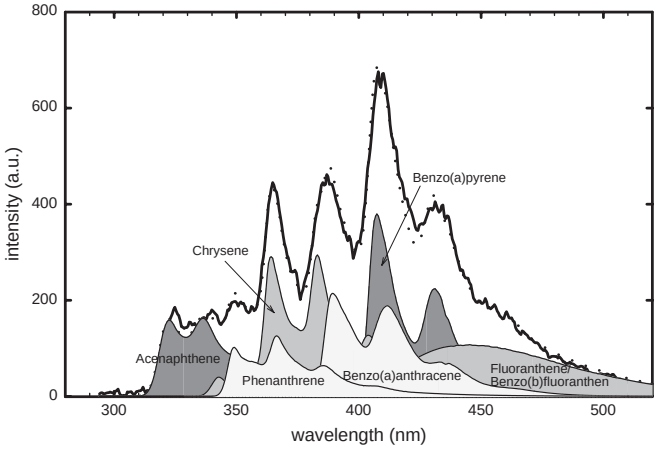

Fig. 10. Component with 23-ns decay time obtained by Knorr–Harris fit of the US-EPA standard (*solid line*) and spectrum obtained by six component least squares fit to this data (*dotted line*). The individual spectra of the six PAHs are shown below. Excitation wavelength: 266 nm

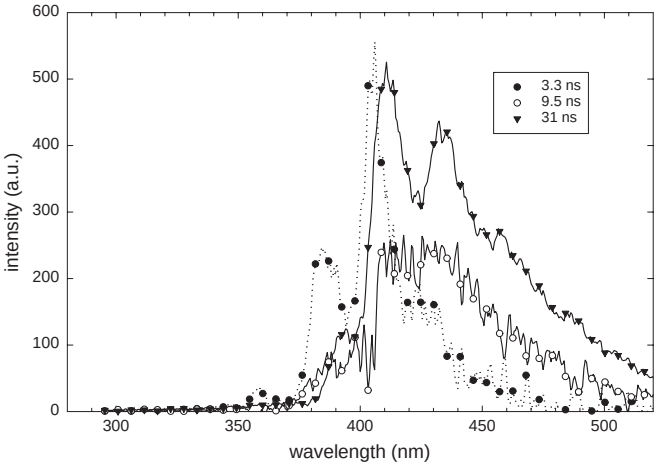

Fig. 11. Plot of the three components obtained by a Knorr–Harris fit applied to the time-resolved spectrum of the US-EPA 610 standard. Excitation wavelength: 355 nm

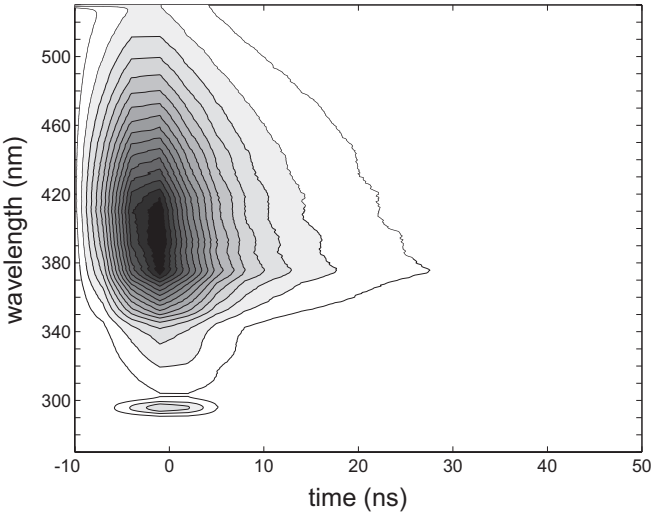

Fig. 12. Contour plot of the time-resolved fluorescence spectrum of a sample from a gasworks location. Excitation wavelength: 266 nm

pounds is easier in this case. The shortest decaying component with a 3.3 ns decay time is anthracene with its typical peaks, although the 370-nm peak is attenuated by the cut-off filter for stray light rejection. The second component with 9.5 ns can be assigned to benzo(k)fluoranthene according to its decay time, although the signal is weak and not very structured. The third component with a 31 ns decay time consists mainly of benzo(a)pyrene with its typical peaks and of benzo(b)fluoranthene/fluoranthene fluorescence with the broad shoulder from 450 to 500 nm.

These results show the potential of the method for the identification of single compounds in complex mixtures. In order to get concentration values of the components, it is necessary to perform a multivariate calibration with a set of known mixtures before.

3.1 Spectra of contaminated water samples

We further investigated samples of polluted water. The first sample originates from a former gasworks location where tar contamination is present. Therefore the sample was expected to contain large amounts of PAHs. A liquid sample was prepared by solving a part of the solid sample using acetonitrile in water. The contour plot of the time-resolved spectrum of this sample with 266-nm excitation is shown in Fig. 12. A broad background fluorescence dominates the spectrum at first glance, but obviously some components with longer decay times are contained in the sample as well. Especially pyrene with a very long decay time of 122 ns and a double peak at 370/390 nm is supposed to be present. It is likely that some of the other larger PAHs are also present, due to the prolonged decay times in the wavelength range from 340 to 480 nm. Smaller PAHs with shorter wavelength fluorescence cannot be found, which confirms the expectation of a sample where tar is the dominating pollutant.

The next sample is groundwater polluted from an accident at a petrol station. The contour plot is shown in Fig. 13, where again 266 nm is used as the excitation wavelength. Contrary to case for the previous sample, short wavelength fluorescence from 280 to 340 nm is also present here together with

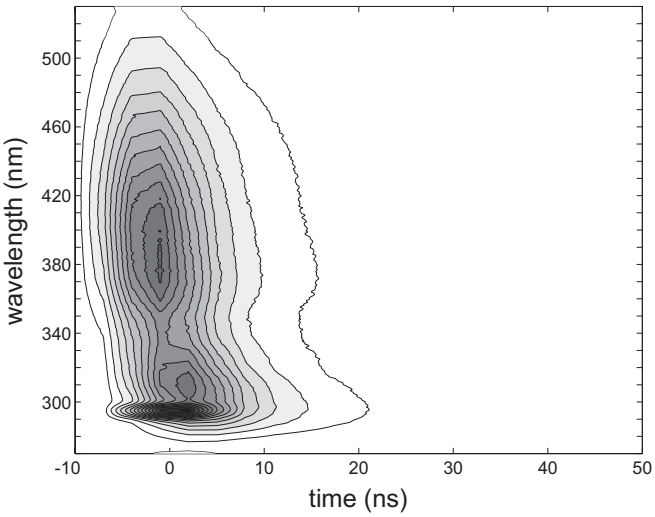

Fig. 13. Contour plot of the time-resolved fluorescence spectrum of a groundwater sample obtained after an accident at a petrol filling station. Excitation wavelength: 266 nm

rather unstructured fluorescence from 340 to 500 nm. The pollution is obviously dominated by BTXE molecules, which show fluorescence in the short wavelength range. Larger molecules seem to play a minor role. This result is what we expected since in the case of an accident, the better soluble compounds, i.e. the BTXE and smaller PAH molecules, reach the groundwater first, whereas the larger molecules, if present at all, are retained by the soil. In the case of the petrol station accident, probably only the smaller molecules were present.

In order to get more information about what happens after a gasoline spill, we contaminated water with a trace of petrol. In the time-resolved fluorescence spectrum of the water only short wavelength fluorescence can be found (see Fig. 14). Apart from the BTXE fluorescence, a longer decaying component with a double peak at 320/340 nm is also present due to naphtalene/acenaphtene. Thus for this kind of pollution, the short excitation wavelength of 266 nm proves to be very advantageous.

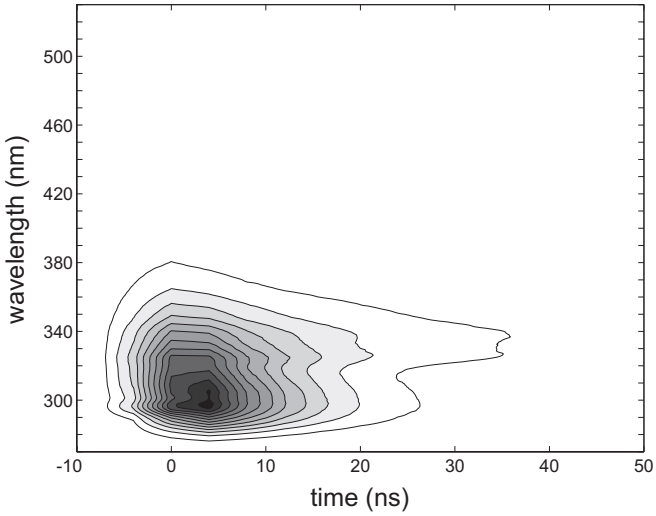

Fig. 14. Contour plot of the time-resolved fluorescence spectrum of petrol dissolved in distilled water. Excitation wavelength: 266 nm

4 Conclusion

By developing a dedicated diode-laser-pumped solid-state laser, the construction of a compact, battery powered LIF system was possible. Two excitation wavelengths (266 nm and 355 nm) can be used alternately. The 266 nm is perfectly suited for the detection of monoaromatics (BTXE) and small PAHs, whereas 355 nm is preferable for a more selective excitation of larger PAHs.

By exploiting the different fluorescence decay behavior, it is possible to group the PAHs according to their fluorescence lifetimes, which facilitates a multicomponent analysis. This promising approach will be extended to the quantitative analysis of aromatic molecules in natural samples.

The measurements from two real-world samples (gas-work, petrol station) reveal that the type of contamination can easily be distinguished with our system. Further research is directed to automatical classification of the kind of pollution and a quantification.

Acknowledgements. Financial support by the Deutsche Bundesstiftung Umwelt (grant no. 01989) and the German Bundesministerium für Bildung, Wissenschaft, Forschung und Technologie (grant no. 16 SV 558/0) is gratefully acknowledged.

References

1. J.E. Kenny, G.B. Jarvis, W.A. Chudyck, K.O. Pohlig: Anal. Instrum. **16**, 423 (1987)
2. S.M. Inman, P. Thibado, G.A. Theriault, S.H. Lieberman: Anal. Chim. Acta **239**, 45 (1990)
3. U. Panne, F. Lewitzka, R. Niessner: Analusis **20**, 533 (1992)
4. P. Karlitschek, U. Bünting, T. Nörthemann, G. Hillrichs: SPIE Proc. **2965**, 88 (1996)
5. G. Hillrichs, W. Neu: "UV laser induced fluorescence to determine organic pollutions in water", Laser in Remote Sensing, ed. by C. Werner, W. Waidelich (Springer, Berlin, Heidelberg 1993) pp. 109-112
6. W. Schade, J. Bublitz, V. Helbig, K.-P. Nick: "Time-resolved laser-induced fluorescence spectroscopy for diagnostics of oil-pollution in water", Laser in Remote Sensing, ed. by C. Werner, V. Klein, K. Weber (Springer, Berlin, Heidelberg 1991) pp. 53-61
7. J. Bublitz, M. Dickenhausen, M. Grätz, S. Todt, W. Schade: Appl. Opt. **34**(18), 3223 (1995)
8. M.U. Kumke, H.-G. Löhmannsröben, Th. Roch: J. Fluoresc. **5**(2), 139 (1995)
9. G.A. Theriault, R. Newbery, J.M. Andrews, S.E. Apitz, S.H. Lieberman: SPIE **1796**, 115 (1992)
10. I.B. Berlman: Handbook of Fluorescence Spectra of Aromatic Molecules (Academic Press, New York 1971)
11. H. Fabian, U. Grzesik, G. Hillrichs, W. Neu: SPIE **1893**, 24 (1993)
12. G. Hillrichs, M. Dressel, H. Hack, R. Kunstmann, W. Neu: Appl. Phys. B **54**, 208 (1992)
13. M. Dressel, W. Neu, H. Gerhardt: Laser Optoelektron. **22**(5), 76 (1990)
14. P. Karlitschek, G. Hillrichs, K.F. Klein: Opt. Commun. **116**, 219 (1995)
15. G. Hillrichs, P. Karlitschek, W. Neu: SPIE **2293**, 178 (1995)
16. T.Y. Fan, R.L. Byer: IEEE J. Quantum Electron. **QE-24**(6), 895 (1988)
17. P. Karlitschek, G. Hillrichs: Appl. Phys. B **64**, 21 (1997)
18. H.R. Verdun, T. Chuang: Opt. Lett. **17**(14), 1000 (1992)
19. U. Bünting, P. Karlitschek: accepted by Spectrochim. Acta A
20. F.J. Knorr, J.M. Harris: Anal. Chem. **53**, 272 (1981)
21. A.L. Wong, J.M. Harris: Anal. Chem. **61**, 2310 (1989)